Open Ceramics 15 (2023) 100379

Contents lists available at ScienceDirect

Open Ceramics

journal homepage: www.sciencedirect.com/journal/open-ceramics

Influence of filter surface roughness on the pressure drop of ceramic foam filters

Claudia Voigt [a,*], Eric Werzner [b], Robert Fritzsch [c], Jana Hubálková [a], Massoud Hassanabadi [d], Ragnhild E. Aune [c], Murilo D.M. Innocentini [e], Christos G. Aneziris [a]

[a] Technische Universität Bergakademie Freiberg, Institute of Ceramics, Refractories and Composite Materials, Agricolastr. 17, 09599, Freiberg, Germany
[b] Technische Universität Bergakademie Freiberg, Institute of Thermal Engineering, Chair of Gas and Heat Technology, Gustav-Zeuner-Str. 7, 09599, Freiberg, Germany
[c] Department of Materials Science and Engineering, Norwegian University of Science and Technology (NTNU), Trondheim, Norway
[d] Innovation & Technology, Hydro Extruded Solution AB, Kanalgatan 1, Finspång, Sweden
[e] University of Ribeirão Preto, Course of Chemical Engineering, Ribeirão Preto, SP, Brazil

ARTICLE INFO

Handling Editor: Dr P Colombo

Keywords:
Open-cell ceramic foam
Alumina
Pressure drop
Surface roughness
Permeability

ABSTRACT

The pressure drop of a ceramic foam filter is an important characteristic indicating the resistance to fluid flow through the filter. Filtration experiments have shown that filtration efficiency increases with decreasing functional pore size. However, this improvement comes at the cost of a higher pressure drop. Furthermore, trials with increased roughness of filter struts showed an improved filtration behavior. Comparing the influence of these filter properties on the filter efficiency is of high interest in terms of filtration per pressure drop. Therefore, the sensitivity of the pressure drop with respect to surface roughness needs to be known. In the study, the pressure drop of ceramic foam filters was measured for different functional pore sizes, porosities, and surface roughness in a water-based test facility at NTNU in Trondheim, Norway. The flow velocity was varied in the range of 0.6–80 cm/s, allowing the determination of the Darcy and non-Darcy permeability coefficients.

1. Introduction

Ceramic foams are used in the area of metal melt filtration for conditioning the melt flow and the removal of non-metallic inclusions [1]. According to Damoah et al. [2], the filtration efficiency of ceramic foam filters (CFFs) depends on various melt parameters (temperature, viscosity, and composition), process parameters (filtration rate, melt pretreatment, and design of the casting system), inclusion parameters (chemism, microstructure, size, and number), and filter parameters (geometry, porosity, chemism, wetting behavior, size, and distribution of functional macropores). For an existing industrial casting process, most of the mentioned parameters are difficult to adjust, except for the parameters of the filter, which can be configured easily. Hence, efforts to improve filtration efficiency are focused on the parameters of the filter. Most geometrical features of filter structures that are beneficial for filtration (e.g., high ppi (pores per inch) number, low porosity, or presence of closed windows) are associated with an increased pressure drop [3,4]. A higher pressure drop is detrimental to the financial viability and operational reliability of the filtration process. Such filters demand a higher pressure head or pumping power to maintain a desired flow rate.

Furthermore, a low pressure drop is essential for the priming process of CFFs. During priming, the Laplace pressure and a higher melt viscosity (due to cooling effects) may additionally increase the flow resistance and raise the risk of melt freezing. Besides the macroscopic geometry of the filter, its wetting behavior also strongly depends on its surface roughness, which may play an important role during filtration. Previous studies conducted by the cooperative research center 920 (Multifunctional Filters for Metal Melt Filtration - a Contribution to Zero Defect Materials) using a water-based model indicated increased adhesion forces between non-metallic inclusions and the filter wall with increasing surface roughness [5,6], suggesting a positive effect on filtration. Industrial-scale filtration trials and LiMCA analyses at Hydro (Bonn, Germany) conducted by Voigt et al. [7] using modified filters and liquid aluminum showed positive contributions of (higher) surface roughness values on the filter performance as well. Nevertheless, recent filtration trials at Hydro Aluminium ASA (Sunndalsøra, Norway) using similarly modified filters could not reproduce comparable results [8]. However, SEM investigations of the used filters showed a very low amount of typical non-metallic inclusions, which may have resulted in

* Corresponding author.
E-mail address: Claudia.voigt@ikfvw.tu-freiberg.de (C. Voigt).

https://doi.org/10.1016/j.oceram.2023.100379
Received 14 April 2023; Received in revised form 22 May 2023; Accepted 24 May 2023
Available online 1 June 2023

the described filtration behaviour. Further trials are necessary to understand the filtration behaviour considering the effect of surface roughness on the filtration performance.

The junior research group PurCo funded by the BMBF (Federal Ministry of Education and Research) do research to understand whether the enhancement of surface roughness for improved filtration is advantageous. The resulting pressure drop and its influence on the flow resistance has to be understood. While the effect of the ppi number on the filtration efficiency [2,9] and pressure drop [10–12] has been extensively studied, the effect of filter roughness on flow resistance has not yet been reported for CFFs. In the area of flow behavior in pipes or packed bed reactors, there are investigations on the influence of interfacial surface roughness. For instance, it is well-known that the friction factor of turbulent pipe flow increases with increasing pipe wall roughness. To a lesser extent, this effect also occurs for laminar pipe flow [13]. Concerning flows through packed beds, different opinions can be found in literature. According to Eisfeld [14], there is no significant influence of particular surface roughness on the pressure drop in a packed bed reactor. In contrast, Crawford et al. [15] experimentally detected an increase in the pressure drop with increasing roughness of the spheres in a packed bed reactor for Reynolds numbers ranging from 10 to 1600.

To investigate the effect of surface roughness on the pressure drop during the flow of liquid metals through CFFs and to assess its magnitude compared to other geometrical modifications, an experimental study using CFFs with different surface roughness values, porosity, and ppi number was conducted. In this context, several challenges had to be addressed: 1) high temperatures and limited accessibility associated with the handling of liquid metals, 2) small measurable pressure differences due to the high permeability of CFFs, 3) relatively high sample-to-sample variability of the filter geometry, and 4) modification of the surface roughness, e.g., through a coating, without affecting the macroscopic geometry. The last point demands particular attention since the pressure drop in CFFs is very sensitive to porosity, as previously shown numerically [16] and experimentally [12]. In the present study, the pressure drop experiments were performed using water instead of liquid metal. After dividing the pressure drop $\mathrm{d}p$ by the sample thickness, the pressure gradient $\mathrm{d}p/\mathrm{d}x$ was obtained. The measured flow velocities and pressure gradients were later used to evaluate the Darcy and non-Darcy permeability coefficients. These coefficients permitted the estimation of the pressure drop for any flow medium, assuming the Darcy-Forchheimer law to be valid, as described in Eq. (1) [17]:

$$\frac{\mathrm{d}p}{\mathrm{d}x} = \underbrace{\frac{\mu}{k_1}u}_{\text{viscous losses}} + \underbrace{\frac{\rho}{k_2}u^2}_{\text{inertial losses}} \tag{1}$$

where μ is the dynamic viscosity, ρ the density of the fluid, u the superficial velocity. k_1 and k_2 are the Darcy and non-Darcy permeability coefficients, respectively. It should be mentioned that k_2 is also known in literature as the Forchheimer coefficient or inertial permeability. It is important to note that k_1 and k_2 are purely geometrical constants that are independent of fluid properties. Physics-based modeling has shown that k_1 depends on the specific surface area and the length scale of viscous shear, while k_2 responds to the specific cumulative area that the struts project into flow direction [18]. Equation (1) accounts for two effects, causing pressure drop in porous media. At very low velocities, for which u^2 becomes negligibly small, the viscous losses induced by skin friction on the surface of the filter struts are dominating. At high velocities, inertial losses are predominant, i.e., the pressure differences between the upstream and downstream face of the struts, caused by the sudden deceleration of the fluid when approaching the strut. These regimes are known as Darcy and Forchheimer flow, respectively, and surface roughness is expected to affect them differently. In order to identify the flow regime for a given application, the Reynolds number based on the length scale k_1/k_2 is proposed, which is also known as the Forchheimer Fo number [19]:

$$Fo = \frac{\rho u k_1}{\mu k_2} \tag{2}$$

By reformulating Eq. (1) using the Forchheimer number, an expression for the inertial contribution to the total pressure drop χ is obtained as follows:

$$\chi = \frac{Fo}{1+Fo} = \begin{cases} < 0.01 & \text{Darcy flow} \\ 0.01 - 0.99 & \text{intermediate regime} \\ > 0.99 & \text{Forchheimer flow} \end{cases} \tag{3}$$

According to Eq. (3), the transition between the viscous-dominated and inertia-dominated regimes occurs at $Fo = 1$, where inertial losses contribute to 50% of the total pressure drop. For $Fo < 0.01$, inertial losses are smaller than 1%; thus, inertial effects can be neglected, while at $Fo > 100$, inertial losses cover more than 99% of the total losses, allowing the viscous effects to be neglected. If these conditions are met, only one of two permeability coefficients needs to be known to predict the pressure drop. Otherwise, pure Darcy flow prevails for centrifugal filtration by means of filters with extremely high ppi numbers (100 ppi or higher) [20] in the field of metal melt filtration. However, most metal melt filtration processes are situated in the intermediate flow regime, requiring the knowledge of both k_1 and k_2.

2. Materials and methods

2.1. Preparation of ceramic foam filters

Ceramic foams made of alumina (Al_2O_3) were used in the present study, their approximate sintered sizes being 50 mm x 50 mm at a height of 20 mm. For the preparation of the ceramic skeleton foams, polymeric foams and ceramic slurries were needed. The commercial polyurethane foams (Eurofoam, Germany) had ppi numbers between 10 and 40.

The polyurethane foams were coated in a two-step procedure. The polyurethane foams were dipped into slurry 1 (see Table 1), followed by the removal of the excess slurry through a spinning process using a modified stirrer RZR 2102 control mixer (Heidolph, Germany). After drying the foams coated in slurry 1 at room temperature for at least 24 h, the process was repeated with slurry 2 (see Table 1). The rotation speed was set between 500 and 1000 rpm, depending on the used slurry and the ppi number of the polyurethane foams. The centrifugation process took at least 5 s. The solid contents of the Al_2O_3 slurries are given as a range (in Table 1) due to the necessity to adjust the slurry rheology to the ppi numbers of the polyurethane foams. After drying the second coating, a sintering step with a maximum temperature of 1600 °C and a holding time of 2 h followed.

Subsequently, the sintered Al_2O_3 skeleton foams were coated applying the combined dip-centrifugation procedure with different slurries (see Table 2) to obtain different foam surface roughness values.

Table 1
Composition and sintering temperature for preparing the Al_2O_3 skeleton foams (* based on the sum of solids).

	Al_2O_3	
	Slurry 1	Slurry 2
Al_2O_3 CT 9 FG (Almatis, Germany) (mass%)	33.3	
Al_2O_3 CT 3000 SG (Almatis, Germany) (mass%)	33.3	
Al_2O_3 T60/T64 45 μm (Almatis, Germany) (mass%)	33.3	
Thickener Axilat RH 50 MD* (C.H. Erbslöh, Germany) (mass %)	0.5	0
Binder Optapix AC 170* (Zschimmer & Schwarz, Germany) (mass%)	1.0	
Dispersant Dolapix CE 64* (Zschimmer & Schwarz, Germany) (mass%)	0.6	
Solid content (mass%)	80–85	
Sintering temperature of the coating (°C)	1600	

Table 2
Composition of coating slurries for generating different foam surface roughness values (* based on the sum of solids).

	Slurry reference	Slurry 33 μm	Slurry 70 μm
Al_2O_3 CT 9 FG $d_{50} = 5$ μm (Almatis. Germany) (mass%)	33.3		
Al_2O_3 CT 3000 SG $d_{50} = 0.8$ μm (Almatis, Germany) (mass%)	33.3	50	50
Al_2O_3 T60/T64 -45μm (Almatis, Germany) m(mass%)	33.3		
Al_2O_3 P6 $d_{50} = 33$ μm (Almatis, Germany) (mass%)		50	
Al_2O_3 WRA $d_{50} = 70$ μm (Almatis, Germany) (mass%)			50
Thickener Axilat RH 50 MD* (C.H. Erbslöh, Germany) (mass%)		0.5	0.5
Binder Optapix AC 170* (Zschimmer & Schwarz, Germany) (mass%)	1.0		
Dispersant Dolapix CE 64* (Zschimmer & Schwarz, Germany) (mass%)	0.6		
Solid content (mass%)	80–85	44–50	44–50

The slurries '33 μm' and '70 μm' are named according to the d_{50} of the raw material with the largest particle size. The filters coated in these slurries were labeled in the same way – 'reference filter', 'filter 33 μm', and 'filter 70 μm'. After drying and sintering at 1600 °C, the ceramic foam surface was evaluated using a digital optical microscope VHX-2000 (Keyence Cooperation, Japan) and a VK-X 1000 laser scanning microscope (Keyence Cooperation, Japan). Improving visibility of the filter surface quality, a surface shape correction (waveform removal) was set to remove the height differences. Furthermore, the strut thickness and window size of the 10 ppi, 20 ppi, 30 ppi, and 40 ppi reference ceramic foam filters were measured with a digital microscope VHX-2000D (Keyence, Japan). At least 50 struts and windows per filter type were analyzed.

In addition to the ppi numbers of the filters, their porosity plays an important role in measuring the pressure drop as the filter porosity has a direct effect on their permeability. Considering the filter mass, a bulk density of the struts equal to $\rho_{struts} = 3.1$ g/cm^3 (measured by mercury intrusion porosimeter Autopore 5 (Micromeritics, USA)) and the calculated volume of the ceramic foam V_{filter} (length · width · height of the filter), the filter strut volume V_{struts} and the porosity ε can be calculated:

$$V_{struts} = \frac{\rho_{struts}}{m_{filter}} \tag{4}$$

$$\varepsilon = 1 - \frac{V_{struts}}{V_{filter}} \tag{5}$$

2.2. Measurement of pressure drop

The pressure drop was determined using a water-based test facility at the Norwegian University of Science and Technology (NTNU, Trondheim, Norway). A filter holder made of acrylic glass was used to keep the filter in place in the water channel. For each measurement of rectangular samples, a sample holder with rectangular openings of 47.5 × 47.5 mm^2 was used, and two rectangular filters were stacked above each other. The sealing of the filters required extra attention to avoid bypassing of water during the experiments. Grease impregnated (high vacuum grease, Dow Corning, USA) cellulose fibers were used to block the pores of the filter sidewalls, closing the space between the filter holder and the filter. The filter holder was connected to a water tank (970 × 670 × 1000 mm^3) filled with 500 l of tap water at 16 °C. The connection is made through smooth pipes with an inner diameter of 49.8 mm, which extended 1250 mm in both upstream and downstream directions, providing a development length of 25 diameters. A vertical multistage centrifugal pump (maximum pressure 10 bar) with an integrated frequency converter (Grundfos, Denmark)) was applied to pump the water. The flow velocities varied between 0.006 m/s and approx. 0.8 m/s, using different valve settings (low flow velocities) and different power levels of the pump (high flow velocities). The flow velocity was indirectly determined from the mass gain using a scale (Flintab, Germany) that recorded the mass of the water collected at the outlet at intervals of 1 s. Once 20 values were recorded, the mass flow rate $\dot{m}$ (kg/s) was calculated, and the corresponding velocity u was determined:

$$u = \frac{\dot{m}}{\rho_{water} \bullet \pi \bullet r_{tube}^2} \tag{6}$$

A density value of $\rho_{water} = 998.9$ kg/m^3 (16 °C) and a radius r_{tube} of 24.9 mm were used.

The pressure drop was measured using a differential pressure transducer (AEP, DF2R, Italy). The transducer had a measuring range of 0–1 bar, at an error ±0.04%, specified by the manufacturer. At the beginning of each measurement series, a taring was performed. The 4–20 mA output signal of the transducer was recorded with a digital multi-meter (FLUKE 289 True RMS Multimeter, USA) and converted to pressure values according to the specifications of the manufacturer. For each flow velocity, an average of 20 individual electrical current measurements was calculated. In order to obtain the pressure gradient, the pressure drop was divided by the height of the ceramic foam filter. After the assembly of the filter into the measurement system, the pump was started with maximum pressure for approximately 15 s to fill the system with water and to remove the air bubbles from the system.

2.3. Determination of Darcy and non-Darcy permeability coefficients

The Darcy and non-Darcy permeability, k_1 and k_2, respectively, were evaluated by fitting the measured pressure gradient using the Darcy-Forchheimer law, as given in Eq. (1), considering the aforementioned water density and a dynamic viscosity of $\mu = 1.108$ mPa·s. The coefficients k_1 and k_2 were obtained by a least-square minimization of the relative error after excluding obvious outliers. Fig. 1 shows an example fit for one of the 30 ppi foam samples, for which an average relative deviation from the experimental data of 2% was determined. Across all foam samples, the average error varied between 2% and 10%. The error was found to increase for filters with small ppi numbers and low velocities, for which the pressure drop became very small. As seen in Fig. 1, all data points are located in the intermediate flow regime, and only a few cover viscous-dominated flow, i.e., $Fo < 1$, which further increases the uncertainty for the prediction of k_1. It should be mentioned that the Darcy-Forchheimer law is not strictly valid in the intermediate region [21]. The determined permeability coefficients should therefore only be considered estimates.

In order to check the procedure, we compared our results with a comprehensive literature collection of Darcy and non-Darcy permeability coefficients for different types of porous media, including many CFFs. The comparison presented in Fig. 2 reveals good agreement in terms of the variation of k_2 with k_1. Furthermore, the obtained results are reasonably well predicted by a fit that was obtained for the complete data collection:

$$k_2 = \exp\left(-1.71588 k_1^{-0.08093}\right) \tag{7}$$

This equation can be used further to estimate k_2 if k_1 is known or vice versa:

$$k_1 = \left(-\frac{1.71588}{\ln(k_2)}\right)^{12{,}3564} \tag{8}$$

3. Results and discussion

3.1. Sample characterization

Micrographs of the prepared ceramic foams were captured by different digital microscopes at different magnifications to get a visual

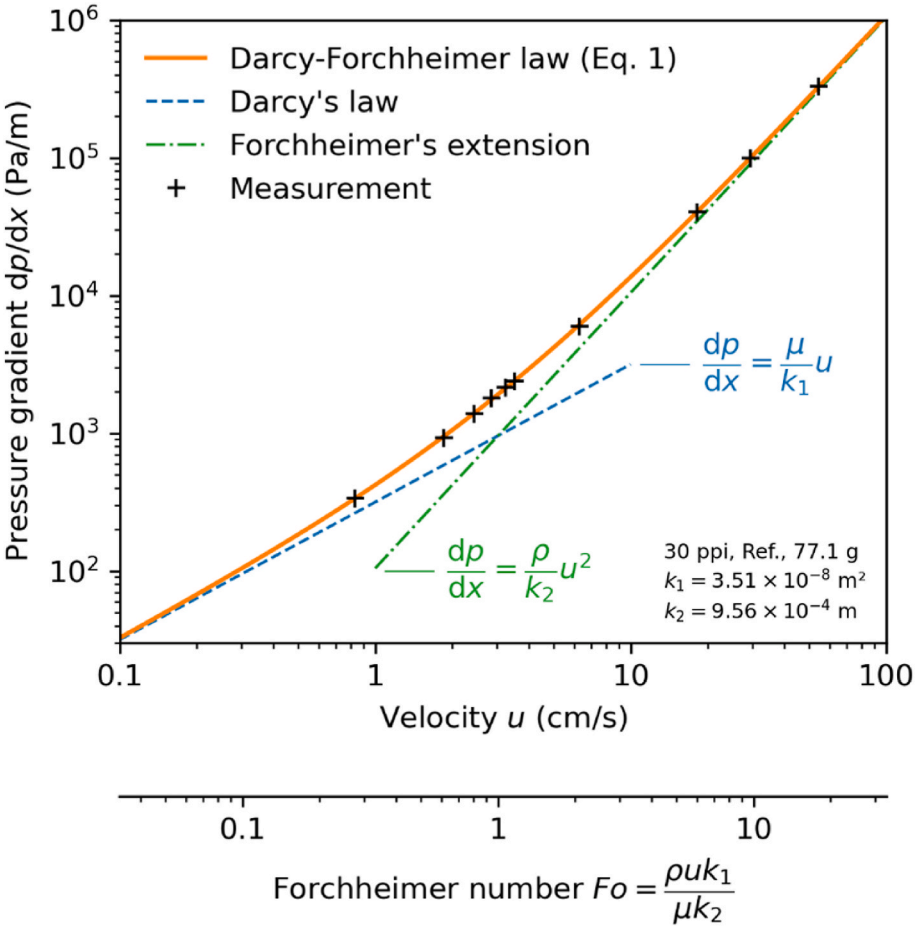

Fig. 1. Determination of the Darcy and non-Darcy permeability by fitting the measured pressure gradient with flow velocity using the Darcy-Forchheimer law. The dashed and dash-dotted lines are the asymptotes for the pure Darcy and Forchheimer regimes, respectively.

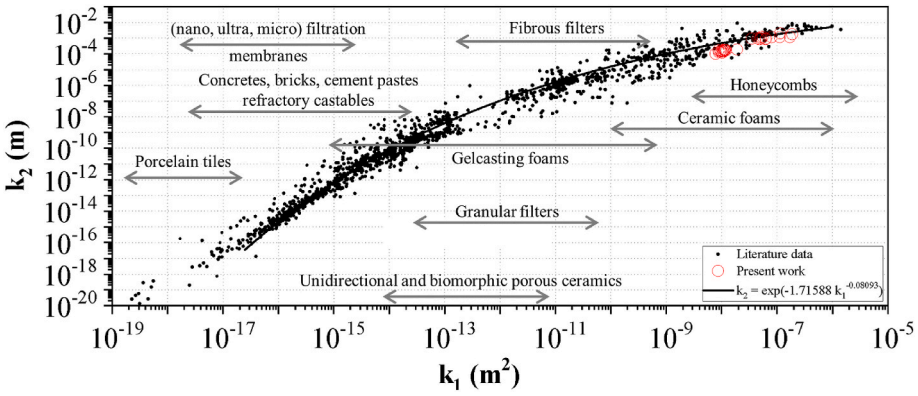

Fig. 2. Variation of the Darcy permeability k_1 with respect to the non-Darcy permeability k_2 based on literature data [17] and data from the present study.

impression of the different ppi numbers (Fig. 3) and filter surface roughness variations (Fig. 4). With an increasing ppi number, the functional pore size decreased, and the amount of closed windows increased. The application of slurries with different particle size distributions significantly influences the filter surface roughness, as seen in Fig. 4. The reference ceramic foam filters (Fig. 4 a and d) coated in the slurry reference show a smooth surface, comparable to commercially produced ceramic foam filters. On the other hand, the filter coated in 33 μm slurry (Fig. 4 b and e) features a very rough surface, whereby the coating seems to be distributed homogenously. It should be noted that the images were taken from the filter surfaces. Therefore, no statement can be made on the distribution of the coating within the filter. The filter coated in the coarsest particles (70 μm filters) possessed the largest grains at the surface, which were distributed inhomogeneously, see Fig. 4 c and f. The difference between 33 μm and 70 μm filters can be explained by the differences in the centrifugal force used during the spin coating session as the larger particles were hurled out by the centrifugal force resulting in the lower amount of larger particles at the surface.

The strut thickness and window size summarized in Table 3 were measured using a digital microscope. The dimensions, masses, and calculated porosities of the investigated ceramic foam filters are compiled in Table 4. As previously mentioned, a stack of two filters was

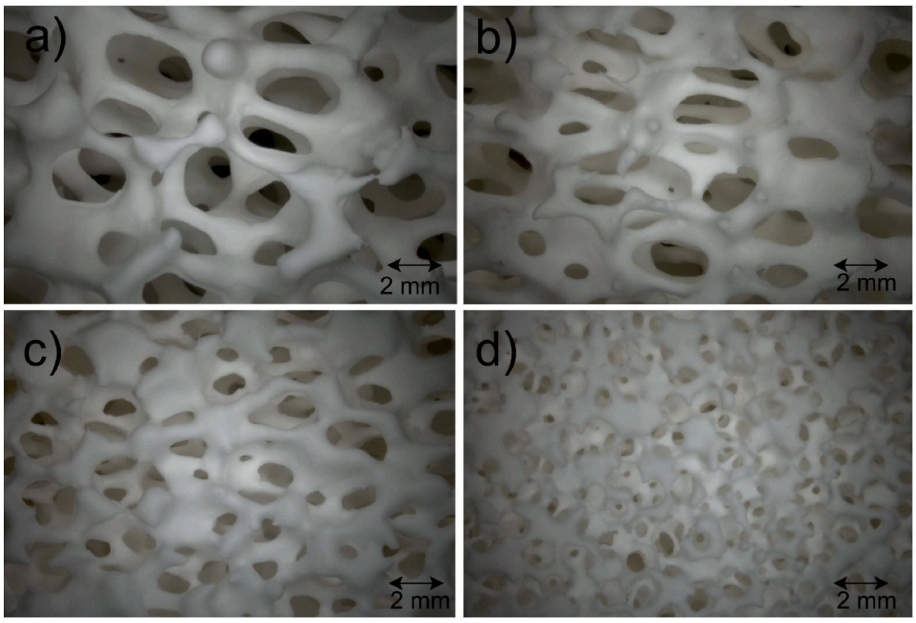

Fig. 3. Photographs of reference filters (rectangular samples) with different ppi numbers: a) 10 ppi, b) 20 ppi, c) 30 ppi, and d) 40 ppi.

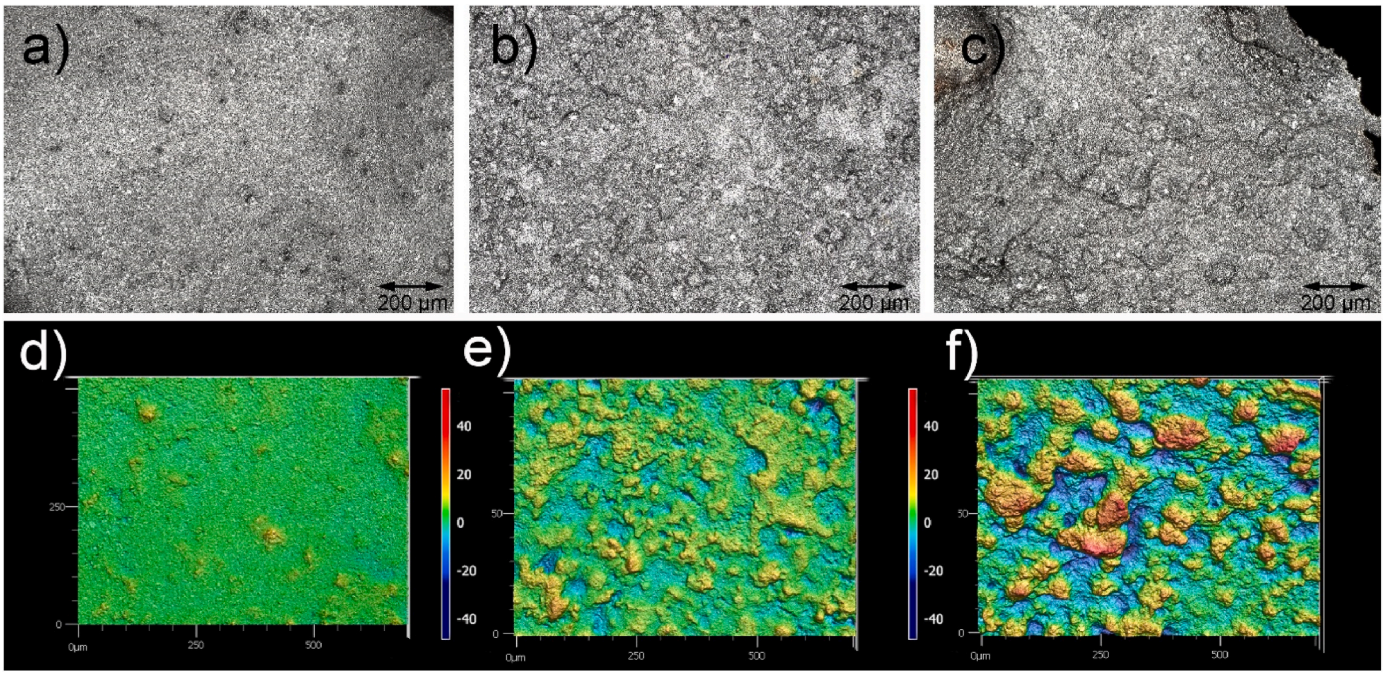

Fig. 4. Laser scanning and surface topography images of 30 ppi filters with different surface roughness values, a) and d) show the reference filter, b) and e) the 33 µm filter, and c) and f) the 70 µm filter.

Table 3
Strut thickness and window size of the Al_2O_3 reference foams (rectangular samples).

	10 ppi	20 ppi	30 ppi	40 ppi
Strut thickness (mm)	0.80 ± 0.21	0.52 ± 0.10	0.49 ± 0.15	0.31 ± 0.07
Window size (mm)	1.46 ± 0.67	1.28 ± 0.54	0.91 ± 0.34	0.55 ± 0.16

used to achieve a higher filter height for the pressure drop measurements of the rectangular ceramic foam filters.

3.2. Pressure drop measurement

Previous pressure drop measurements of cylindrical samples with a diameter of 50 mm and a height of 50 mm showed significant problems with the repeatability for the 30 µm and 70 µm filters. It is suggested that this is the result of the inhomogeneity of filter coatings with larger particles. Increased filter sizes and thicknesses, reduced macro pore sizes and large coating particles (30 µm and 70 µm slurries) result in challenging coating procedures, as the coarse slurry is harder to introduce

Table 4
Dimensions, mass, calculated total porosity, and the Darcy and non-Darcy permeability coefficients k_1 and k_2 of the Al_2O_3 filter foams (?).

ppi	Dimensions of two filters about each other (mm^3)	Surface type	Filter mass			Porosity of filter 1 + 2 (vol%)	k_1 (m^2)	k_2 (m)
			Filter 1 (g)	Filter 2 (g)	Sum (g)			
10	49.7 × 49.9 x 43	Reference	37.7	35.8	73.5	77.8	$1.51{\cdot}10^{-7}$	$1.91{\cdot}10^{-3}$
20	49.5 × 49.3 x 43	Reference	37.5	37.7	75.2	76.9	$1.21{\cdot}10^{-7}$	$(1.18{\cdot}10^{-3}$
30	47.7 × 48.0 x 42.2	Reference	33.6	35.2	68.8	77.5	$5.51{\cdot}10^{-8}$	$1.20{\cdot}10^{-3}$
	47.3 × 47.9 x 42.8	Reference	35.4	36.5	71.9	76.1	$5.07{\cdot}10^{-8}$	$1.19{\cdot}10^{-3}$
	47.8 × 47.9 x 43.0	Reference	37.7	38.1	75.8	75.2	$5.33{\cdot}10^{-8}$	$9.57{\cdot}10^{-4}$
	48.0 × 47.1 x 42.6	Reference	38.1	39	77.1	74.2	$5.51{\cdot}10^{-8}$	$9.56{\cdot}10^{-4}$
	47.6 × 47.1 x 42.5	33 μm	37.7	38	75.7	74.4	$4.83{\cdot}10^{-8}$	$8.81{\cdot}10^{-4}$
	47.7 × 47.1 x 42.5	70 μm	37.7	37.5	75.2	74.6	$6.22{\cdot}10^{-8}$	$8.59{\cdot}10^{-4}$
40	50.0 × 50.0 x 44.8	Reference	35.3	35.1	70.4	79.7	$1.89{\cdot}10^{-8}$	$1.94{\cdot}10^{-4}$
	50.1 × 50.2 x 45.3	Reference	38.5	37.5	76.0	78.5	$1.15{\cdot}10^{-8}$	$1.78{\cdot}10^{4}$
	50.0 × 50.3 x 45.2	Reference	44.5	44.7	89.2	74.7	$9.98{\cdot}10^{-9}$	$1.72{\cdot}10^{-4}$
	49.8 × 49.9 x 45.3	Reference	47.3	47.7	95.0	72.8	$7.77{\cdot}10^{-9}$	$1.01{\cdot}10^{-4}$
	50.1 × 49.8 x 45.1	33 μm	37.6	37.9	75.5	78.4	$9.84{\cdot}10^{-9}$	$1.35{\cdot}10^{-4}$
	49.6 × 50.0 x 44.8	70 μm	36.8	38.9	75.7	78.0	$1.06{\cdot}10^{-8}$	$1.45{\cdot}10^{-4}$

into the depth of the foam. For this reason, it was decided to use filters with an easier-to-coat form of approximately 50 × 50 × 20 mm^3. To adjust the filter height, a stack of two filters was used for the pressure drop measurements.

Fig. 5 shows the variation of pressure gradients with velocities for rectangular ceramic foam filters with different ppi numbers, ranging from 10 to 40 ppi, whereby the porosity of the filters was established to be between 75.2% and 78.5%. In Fig. 5 a, logarithmic scales were used on both axes in order to clarify the variations in the low-velocity range, while Fig. 5 b shows linear scales, illustrating the effects at high velocities. The same style was also adopted for the results, presented in the following section. The determination of the pressure drop was repeated at least once, whereby the stacked filters were removed and repositioned between measurements. The measurements show good repeatability, and significant differences in pressure drop values between different ppi numbers were obtained. Overall, it was established that the pressure drop was higher for higher ppi numbers. This is an expected result and is in accordance with various publications [10–12].

The influence of the filter porosity on the pressure drop was also investigated for both 30 and 40 ppi filters, as shown in Figs. 6 and 7, respectively. The filter porosity of the stacked filters proved to vary between 74.2% (77 g) and 77.5% (69 g) for the samples with 30 ppi and between 72.8% (95 g) and 79.7% (70 g) for the 40 ppi CFFs. The obtained differences in the pressure drop are believed to be a result of the interlinking of the pressure drop and the filter porosity. For the lower filter porosities, the pressure drop is higher, as the higher strut volume present in these filters acts as a flow resistor. However, it is notable that the obtained pressure drops for CFFs with 40 ppi, of higher filter porosities, i.e., 75%, 79%, and 80%, are relatively close to each other. In comparison, the lowest porosity of 73% (95 g) possesses a significantly higher pressure drop. This is believed to result from the higher proportion of closed pores with decreasing filter porosity.

Overall, the significant influence of filter porosity on the filter performance is clearly shown by the presented experimental data. Therefore, it must be taken into account during the investigation of the effect of filter roughness on the pressure drop.

The pressure drop independence on the surface roughness was measured for 30 ppi (Fig. 8) and 40 ppi (Fig. 9) filters, and showed only small differences between the obtained data for the reference filters and the filters with rougher surfaces. However, the difference was established to increase with an increasing superficial velocity of the fluid medium (water). The pressure drop differences between the reference filters and the filters with rougher surfaces proved to be significantly lower than the differences obtained between the different ppi numbers and filter masses.

Further research will be conducted considering the significance of the observed differences. It is, however, notable that the pressure drop of the 33 μm and 70 μm filters were almost the same even if the grain distribution at the surface was different. The 33 μm filters had small but homogenously distributed grains at their surface whereas the 70 μm filters had larger particle sizes at lower numbers.

3.3. Darcy and non-Darcy permeability

The evaluated Darcy and non-Darcy permeability coefficients k_1 and k_2, respectively, are presented in Fig. 10 for different ppi numbers, porosities, and surface treatments. The results match well with the data reported for CFFs in literature with the same nominal ppi number and similar porosity [17,22]. As can be seen from Fig. 10, the permeability coefficients decrease with the ppi number. With increasing ppi numbers, the surface area also increases and the length scale of viscous shear becomes smaller, promoting viscous losses and causing a reduction of k_1. The decrease in k_2 is attributed to the increase in strut area, projected in the flow direction, determining the inertial losses [18]. A simple

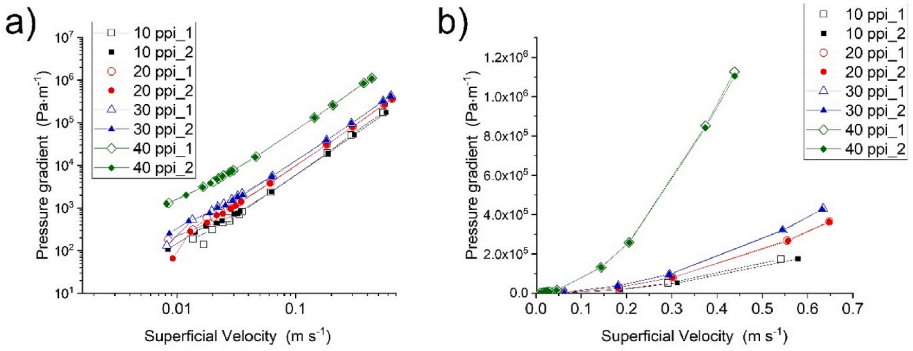

Fig. 5. Pressure drop independence of the superficial velocity for ceramic foam filters of different ppi numbers plotted a) logarithmically and b) linearly.

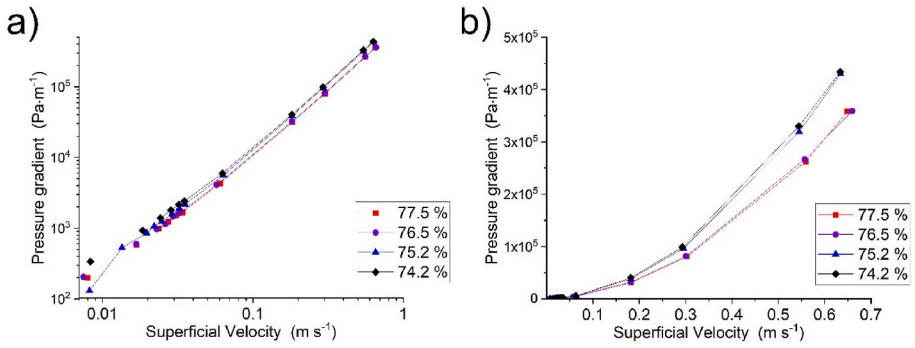

Fig. 6. Pressure drop independence on the superficial velocity and filter porosity of 30 ppi samples plotted a) logarithmically and b) linearly.

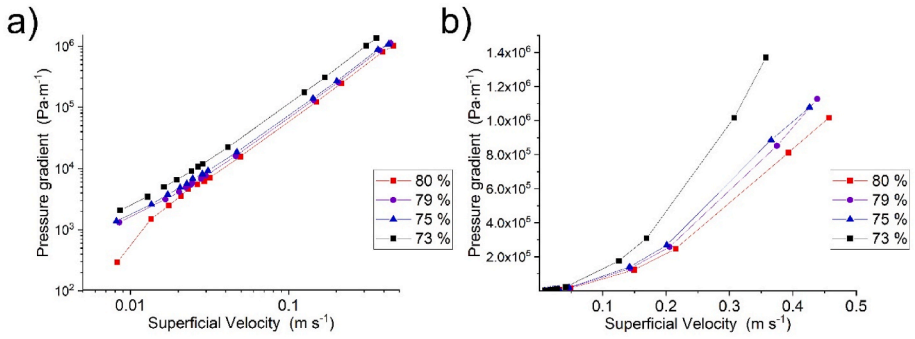

Fig. 7. Pressure drop independence on the superficial velocity and filter porosity of 40 ppi samples plotted a) logarithmically and b) linearly.

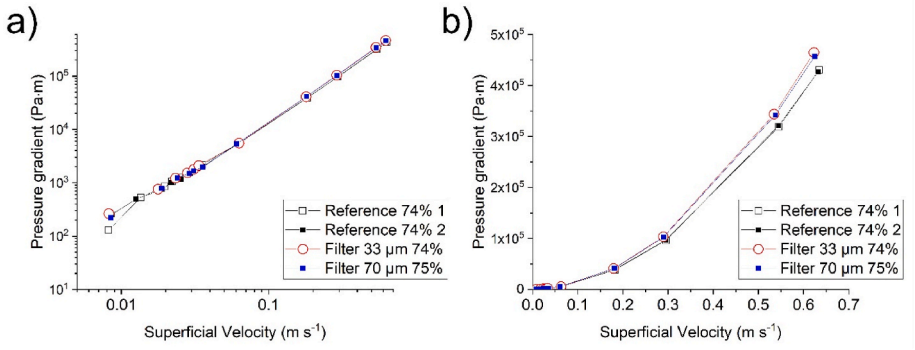

Fig. 8. Pressure drop independence on the superficial velocity of 30 ppi filters with different surface roughness a) logarithmically and b) linearly.

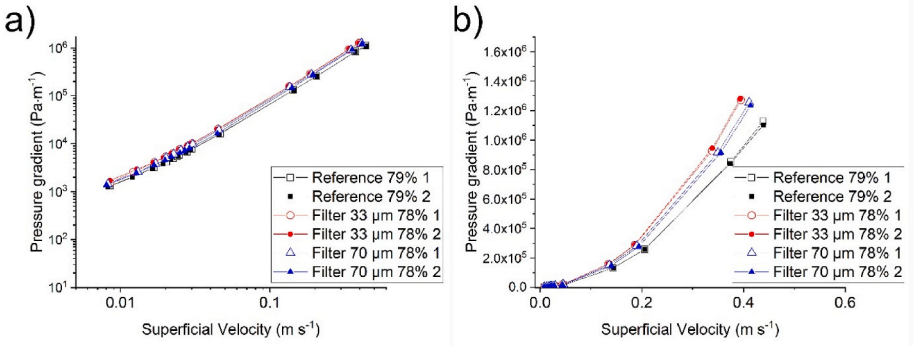

Fig. 9. Pressure drop independence on the superficial velocity of 40 ppi filters with different surface roughness plotted a) logarithmically and b) linearly.

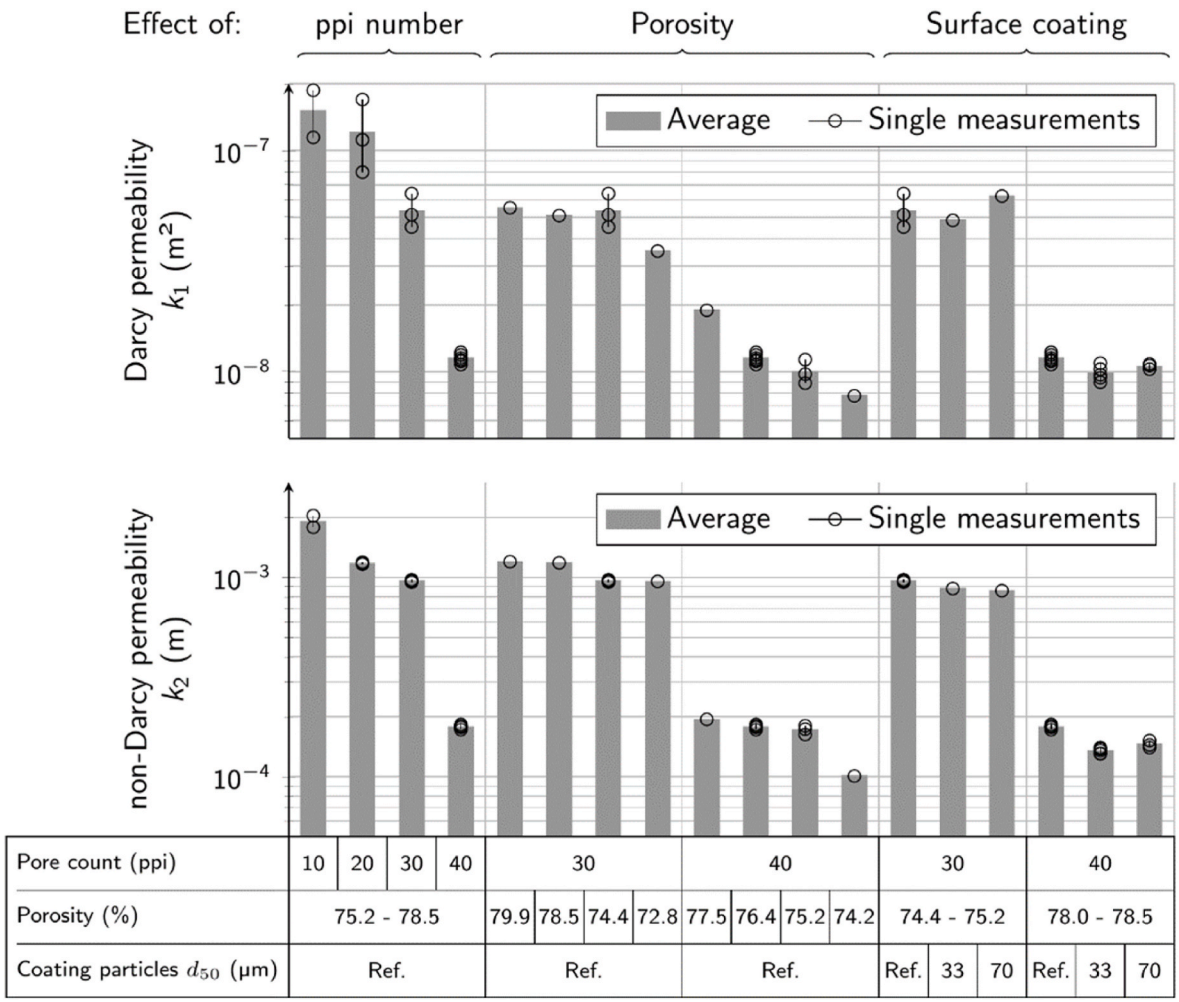

Fig. 10. Variation of the Darcy and the non-Darcy permeability for ceramic foam filters with different ppi number, porosity, and surface coating.

dimensional analysis would suggest scaling relationships in the form of $k_1 \sim \text{ppi}^{-2}$ and, $k_2 \sim \text{ppi}^{-1}$, assuming that the ppi number is an accurate measure of the linear pore density. However, the ppi measure is known to not accurately predict the number of linear pores per inch but rather serves as a rough classification of CFFs. This is also indicated by the non-linear variation of strut thickness and window diameter with the ppi numbers seen in Table 3 and measurements of the pore density reported in literature [16,22]. Therefore, it is not surprising that our results differ from these scaling relationships. In addition, the uncertainty of measurement for k_1 at lower ppi numbers should be taken into account as well as the change of morphological features of the CFFs with ppi number, e.g., the frequency of closed windows or the distribution of filter material between the struts and joints.

The increase in Darcy and non-Darcy permeability with increasing porosity can also be seen in the figure. While literature reports a very high sensitivity for both the k_1 and k_2 coefficients [16,17], this was not consistently reflected by the present results. In particular, the 30 ppi samples exhibit only minor differences with respect to porosity. This observation might be explained by differences in their microstructure. For example, geometrical characteristics, such as the presence of closed windows or non-circular strut cross sections [4], are known to affect k_1 and k_2 differently.

As further shown in the figure, the effect of the surface treatment on the Darcy and the non-Darcy permeability is rather low compared to the influence of the ppi number or the porosity. In case of the 40 ppi samples, the variations of k_1 and k_2 prove to be very similar, with a maximum obtained in both coefficients for the smooth surfaces of the reference filters and the lowest values for the 33 µm filters. Further investigations would be required in order to assess whether such small variations are actually caused by the surface coating or are the effects of sample-to-sample variability in other geometrical characteristics For the sake of completeness, the surface variation is also shown for the 30 ppi samples. However, due to the small number of experimental data, no conclusions can be drawn.

4. Conclusion

The presented investigation was motivated by the fact that the roughness of filter walls has been shown to significantly improve the adhesion forces of inclusions and, thereby, to enhance filtration behavior. However, many measures for improving filtration come at the cost of an increased pressure drop at the used filter. Based on this, the main objective of the present study was to assess the effect of the surface roughness of ceramic foam filters on the pressure drop compared to other geometrical modifications known to promote filtration. This was accomplished by measuring the variations of pressure gradients with respect to velocity, using a water-based test facility for filters with different ppi numbers, porosities, and surface roughness. Subsequently, the Darcy and non-Darcy coefficients were evaluated. The obtained values of the coefficients are in agreement with existing literature data for similar ceramic foam filters and showed the expected trends with respect to the influence of the ppi number and porosity. The surface roughness was, however, found to have only a minor impact on the pressure drop and the permeability coefficients.

Declarations of competing interest

None.

Acknowledgments

The author Claudia Voigt would like to thank the Federal Ministry of Education and Research (BMBF) for supporting these investigations as part of the junior research group PurCo (Project-ID 03XP0420).

The author Eric Werzner would like to thank the German Research Foundation (DFG) for supporting these investigations as part of the Collaborative Research Centre 920 "Multi-Functional Filters for Metal Melt Filtration – A Contribution towards Zero Defect Materials" (Project-ID 169148856) sub-project B02.

References

[1] R.A. Olson III, L.C.B. Martins, Cellular ceramics in metal filtration, Adv. Eng. Mater. 7 (4) (2005) 187–192, https://doi.org/10.1002/adem.200500021.
[2] L.N.W. Damoah, L. Zhang, Removal of inclusions from aluminum through filtration, Metall. Mater. Trans. B 41B (2010) 886–907, https://doi.org/10.1007/S11663-010-9367-3.
[3] C. Demuth, E. Werzner, S. Dudczig, C.G. Aneziris, S. Ray, Large Eddy simulation of turbulent flow and inclusion transport during filtration of liquid steel inside open-cell ceramic foams, Adv. Eng. Mater. (2021), https://doi.org/10.1002/adem.202100717.
[4] H. Lehmann, E. Werzner, A. Malik, M. Abendroth, S. Ray, B. Jung, Computer-aided design of metal melt filters: geometric modifications of open-cell foams, effective hydraulic properties and filtration performance, Adv. Eng. Mater. 24 (2021), 2100878, https://doi.org/10.1002/adem.202100878.
[5] L. Ditscherlein, A. Schmidt, E. Storti, C.G. Aneziris, U.A. Peuker, Impact of the roughness of alumina and Al_2O_3-C substrates on the adhesion mechanisms in a model system, Adv. Eng. Mater. 19 (2017) 9, https://doi.org/10.1002/adem.201700088, 1700088-n/a.
[6] L. Ditscherlein, P. Knüpfer, U.A. Peuker, The influence of nanobubbles on the interaction forces between alumina particles and ceramic foam filters, Powder Technol. 357 (2019) 408–416, https://doi.org/10.1016/j.powtec.2019.08.077.
[7] C. Voigt, M. Dietrich, M. Badowski, M. Gorshunova, G. Wolf, C.G. Aneziris, Impact of the filter roughness on the filtration efficiency for aluminum melt filtration, Light Met. (2019) 1063–1069, https://doi.org/10.1007/978-3-030-05864-7_130.
[8] A. Bergin, C. Voigt, R. Fritzsch, A. Akhtar, L. Arnberg, C.G. Aneziris, R. Aune, Ceramic foam filters (CFFs) during aluminium melt filtration in a pilot-scale setup, Light Met. (2022) 640–648, https://doi.org/10.1007/978-3-030-92529-1_84.
[9] L.J. Gauckler, M.M. Waeber, C. Conti, M. Jacob-Duliere, Ceramic foam for molten metal filtration, J. Met. (1985) 47–50, https://doi.org/10.1007/BF03258640. September.
[10] M. Hassanabadi, M.W. Kennedy, S. Akhtar, R.E. Aune, Verification of experimentally determined permeability and form coefficients of Al_2O_3 ceramic foam filters (CFF) at high and low flow velocity using a CFD model, Extraction (2018), https://doi.org/10.1007/978-3-319-95022-8_69. Springer.
[11] S. Akbarnejad, L.T.I. Jonsson, M.W. Kennedy, R.E. Aune, G.J. P, Analysis on experimental investigation and mathematical modeling of incompressible flow through ceramic foam filters, Metall. Mater. Trans. B 47B (2016) 2229–2243, https://doi.org/10.1007/978-3-319-95022-8_69.
[12] G.I. Garrido, F.C. Patcas, S. Lang, B. Kraushaar-Czarnetzki, Mass transfer and pressure drop in ceramic foams: a description for different pore sizes and porosities, Chem. Eng. Sci. 63 (2008) 5202–5217, https://doi.org/10.1016/j.ces.2008.06.015.
[13] D. Gloss, H. Herwig, Wall roughness effects in laminar flows: an often ignored though significant issue, Exp. Fluid 49 (2010) 461–470, https://doi.org/10.1007/s00348-009-0811-6.
[14] B. Eisfeld, Pseudokontinuierliche Modellierung der Strömung in Schüttschichtreaktoren, Dissertation, Brandenburgische Technische Universitätt Cottbus, 1999.
[15] C.W. Crawford, O.A. Plumb, The influence of surface roughness on resistance to flow through packed beds, ASME J. Fluid Eng. 108 (1986) 343–347.
[16] E. Werzner, M. Abendroth, C. Demuth, C. Settgast, D. Trimis, H. Krause, S. Ray, Influence of foam morphology on effective properties related to metal melt filtration, Adv. Eng. Mater. 19 (2017) 9, 1700240-n/a.
[17] M.D. de Mello Innocentini, P. Sepulveda, F. dos Santos Ortega, in: M. Scheffler, P. Colombo (Eds.), Cellular Ceramics - Structure, Manufacturing, Properties and Applications, Chapter 4.2 Permeability, Wiley-VCH, 2005, pp. 313–341.
[18] P. Jorge, M.A. Mendes, E. Werzner, J.M. Pereira, Characterization of laminar flow in periodic open-cell porous structures, Chem. Eng. Sci. 201 (2019) 397–412.
[19] D. Ruth, H. Ma, On the derivation of the Forchheimer equation by means of the averaging theorem, Transport Porous Media 7 (3) (1992) 255–264.
[20] N. Sun, Z. Wang, B. Sun, Y. Li, Z. Guo, Purification of primary aluminum liquid through supergravity-induced filtration, Chem. Eng. Process Process Intensif. 182 (2022), 109199.
[21] E. Skjetne, J. Auriault, New insights on steady, non-linear flow in porous media, Eur. J. Mech. B Fluid 18 (1) (1999) 131–145.
[22] A. Asad, E. Werzner, C. Demuth, S. Dudczig, A. Schmidt, S. Ray, C.G. Aneziris, R. Schwarze, Numerical modeling of flow conditions during steel filtration experiments, Adv. Eng. Mater. 19 (2017) 9, 1700085-n/a.